Ceramics International 44 (2018) 2745–2751

Contents lists available at ScienceDirect

Ceramics International

journal homepage: www.elsevier.com/locate/ceramint

# Structure, densification and electrical properties of $Gd^{3+}$ and $Cu^{2+}$ co-doped ceria solid electrolytes for SOFC applications: Effects of $Gd_2O_3$ content

Thamyscira H. Santos[a], João P.F. Grilo[b], Francisco J.A. Loureiro[c], Duncan P. Fagg[c], Fábio C. Fonseca[d], Daniel A. Macedo[a,*]

[a] Materials Science and Engineering Postgraduate Program, UFPB, 58051-900 João Pessoa, Brazil
[b] Department of Materials and Ceramic Engineering, University of Aveiro, 3810-193 Aveiro, Portugal
[c] Department of Mechanical Engineering, University of Aveiro, 3810-193 Aveiro, Portugal
[d] Energy and Nuclear Research Institute, IPEN, 05508-170 São Paulo, Brazil

ARTICLE INFO

*Keywords:*
Electrolyte
Gadolinia-doped ceria
Sintering aid
Electrical conductivity

ABSTRACT

Ceria-based solid electrolytes exhibit superior electrical conductivity compared to traditional yttria-stabilized zirconia ceramics. However, they require high sintering temperatures to achieve full densification. Transition metal oxides exhibiting low melting points, such as CuO, have been used as additives to lower the sintering temperature of these materials. In this context, the present work is focused on the evaluation of the effects of gadolinium oxide ($Gd_2O_3$) content on the structure, densification and electrical properties of ceria co-doped with CuO. Nominal compositions of $Ce_{0.99-x}Gd_xCu_{0.01}O_{2-\delta}$ ($0 \leq x \leq 0.3$) were synthesized by the polymeric precursor method. The precursor powders were characterized by simultaneous thermogravimetry and differential thermal analysis (TG/DTA) and the calcined powders were studied by X-ray diffraction (XRD) and Rietveld refinement to obtain crystallographic parameters. The sinterability of green bodies was evaluated by dilatometry up to 1200 °C. The relative density was determined in samples sintered between 950 and 1050 °C and the microstructural characterization was performed by scanning electron microscopy (SEM). The electrical properties were investigated by impedance spectroscopy (IS). The XRD results confirms the formation of a cubic fluorite type structure in the entire composition range. The lattice parameters obtained by Rietveld refinement showed a reduction in the crystallite size with increasing gadolinium content. Densification was improved with increasing Gd-content up to $x = 0.15$. The electrical conductivity was enhanced by gadolinium addition, reaching a maximum of 7.81 mS $cm^{-1}$ at 600 °C for the composition $x = 0.15$ sintered at a temperature as low as 1050 °C.

## 1. Introduction

The development of technological devices aiming to improve human life quality has generated a demand for alternative energy sources, with an intensity never seen before. Currently energy needs are still met by the use of fossil fuels, non-renewable resources that result in high emissions of pollutant gases [1]. In this scenario, solid oxide fuel cells (SOFCs) are regarded a highly attractive method of providing electric power for a sustainable development. Such devices have the capability of producing electricity with high efficiency, accompanied by minimal emission of harmful pollutants. Moreover, they operate without producing noise, with good fuel flexibility and the heat produced during SOFC operation can be used for co-generation to further increase their overall efficiency [2,3]. The basic structure of a SOFC includes a solid ceramic electrolyte sandwiched between two porous electrodes (cathode and anode), combined with interconnectors and sealants. The cathode is fed with an oxidizing gas, promoting oxygen dissociation into $O^{2-}$ ions, while the anode is fed with a combustible gaseous fuel. The electrolyte material carries the oxygen ions from the cathode to the electrolyte/anode interface, where oxidation of the fuel and the formation of electrons (channelled through an external circuit) take place. Water vapor and other by-products (depending on the fuel used) are produced on the anode side [4].

Considering an integrated SOFC system, excess heat from the production of electric current can yield an overall systems efficiency of up to 70% with low $CO_2$ emissions [5]. Nonetheless, the market entry of

* Corresponding author.
*E-mail address:* damaced@gmail.com (D.A. Macedo).

http://dx.doi.org/10.1016/j.ceramint.2017.11.009
Received 11 October 2017; Received in revised form 26 October 2017; Accepted 2 November 2017
Available online 03 November 2017

these devices is still hindered by the high manufacturing cost of the components and their low durability at high operating temperatures, typically between 700 and 1000 °C. To improve longevity, efforts have been made to reduce SOFC operation temperature to the intermediate level, 500–700 °C. However, on such reduction in temperature, selection of component materials becomes critical to avoid efficiency losses related to potentially lowered reaction kinetics of the electrodes as well as increased ohmic resistances of the electrolyte. In the case of the electrolyte, the ohmic losses can be minimised by decreasing thickness and/or by using materials with higher ionic conductivity [6]. The main requirements of an electrolyte material include high densification, high ionic conductivity, good thermal expansion match with other cell components and chemical stability in reducing and oxidizing atmospheres [7,8]. The ionic conductivity of ceria-based solid solutions ($Ce_{1-x}M_xO_{2-\delta}$) is typically maximised through the addition of a suitable aliovalent dopant, such as gadolinium (Gd) or samarium (Sm). In such cases, doping with up to 20 mol% $Gd_2O_3$ increases the ionic conductivity allowing more competitive values to be offered [9,10] than traditional yttria-stabilized zirconia (YSZ) electrolytes in the lower temperature range.

To achieve a dense electrolyte material, ceria-based ceramics are generally sintered between 1400 and 1600 °C. However, such high processing temperatures promote extensive grain growth, which can lead to poor mechanical properties, and can cause undesirable chemical expansion, resulting from the partial reduction of $Ce^{4+}$ to $Ce^{3+}$, which can negatively affect the processing of anode/electrolyte/cathode layers. To overcome these drawbacks, several sintering strategies can be adopted, i.e., reducing the particle size or incorporating a sintering additive. The combination of a fine particle synthesis method, such as the polymeric precursor method, with co-doping with transition metal oxides, such as copper oxide (CuO), has been previously reported to be a good solution to aid the sintering process [11,12]. Moreover, in the development of SOFCs with zirconia/ceria bi-layer electrolytes, lowering the sintering temperature of the ceria diffusion barrier facilitates easy fabrication, lower manufacturing costs and lower reaction with YSZ. Studies on the effect of transition metal doping on CGO ceramics have been done in the case of cobalt addition, highlighted improved densification and a shift in the electrolytic domain of this material in respect to the oxygen partial pressure [13,14]. It was found that the p-type electronic conductivity of CGO ceramics increases on the addition of 2 mol% Co, while the n-type conductivity decreases. This enhancement in p-type conductivity promotes an enlargement of the active electrode surface area at the cathode side leading to a substantial improvement in polarisation behavior [14], while the shifted electrolytic domain remains sufficiently wide for this material to be used as a solid electrolyte for intermediate-temperature electrochemical applications in the operation temperature range 500–700 °C [13,14].

In this scenario, the aim of this work is to evaluate the effect of Gd content on the structure, densification and electrical properties of ceria solid solutions containing 1 mol% CuO as a sintering aid. Solid solutions of nominal composition $Ce_{0.99-x}Gd_xCu_{0.01}O_{2-\delta}$ (x = 0; 0.05; 0.10; 0.15; 0.20; 0.25, 0.30) were synthesized by the polymeric precursor method and investigated by several advanced materials characterization techniques. This study is of a high importance for optimization of the procedure of fabrication of anode-supported SOFCs where the electrolyte should be densified at comparatively low temperatures in order to avoid densification of the supporting porous anode layer [5].

## 2. Experimental

Ceria-based solid solutions with different Gd contents, $Ce_{0.99-x}Gd_xCu_{0.01}O_{2-\delta}$ (x = 0; 0.05; 0.10; 0.15; 0.20; 0.25; and 0.30), co-doped with 1 mol% CuO, were obtained by the polymeric precursor method. The synthesis route comprises the preparation of an aqueous solution of citric acid (Synth, Brazil) at 50 °C, to which nitrates of cerium (Reacton®), gadolinium (Aldrich®) and copper (Aldrich®) were added. Ethylene glycol was then added and the temperature was raised to 75 °C. The resulting gel was thermally treated at 300 °C for 2 h to give the precursor powders.

To evaluate the influence of the gadolinium content on the thermal behavior, the precursor powders were investigated by simultaneous thermogravimetric and differential thermal analysis (TG/DTA) in DTG-60H (Shimadzu) equipment in the 25–1000 °C temperature range, with heating rate of 10 °C $min^{-1}$ and air atmosphere. According to the TG/DTA results, the temperature of 500 °C (with 1 h of dwell time) was adopted for the calcination of precursor powders. The crystalline structure of the calcined powders was analyzed by X-ray diffraction (XRD) in a Shimadzu equipment (model XRD-7000), with a 2θ angular sweep between 20 and 80°, 0.2° step width and a counting time of 2 s per step using a monochromatic Cu $K_\alpha$ radiation (λ = 1.5418 Å) obtained at 40 kV with a filament current of 40 mA. Rietveld refinement of the diffraction data was performed using MAUD software. The standard cards ICSD 72155, ICSD 28795, ICSD 28796, and ICSD 28797 were used to index $CeO_2$, $Ce_{0.9}Gd_{0.1}O_{1.95}$, $Ce_{0.8}Gd_{0.2}O_{1.8}$ and $Ce_{0.7}Gd_{0.3}O_{1.85}$ phases, respectively. Based on the XRD data and Rietveld refinement, the lattice parameters, crystallite size and theoretical density were determined. The values of theoretical density ($\rho_t$) were calculated by the equation:

$$\rho_t = \left(\frac{4}{N_A \bullet a^3}\right)\left[(0.99 - x)M_{Ce} + xM_{Gd} + 0.01M_{Cu} + \left(2 - 0.005 - \frac{x}{2}\right)M_O\right] \quad (1)$$

where "$N_A$" is the Avogadro's number, "$a$" the lattice parameter, "$M$" the atomic mass of each element and "$x$" is the gadolinium content.

For the dilatometric, microstructural and electrical characterization, cylindrical pellets with 10 mm diameter and 2 mm thickness were obtained by uniaxial pressing at 127 MPa. Pellets were sintered in air atmosphere at 1050 °C using a heating rate of 3 °C $min^{-1}$ and a 5 h dwell time. The dilatometric analysis was performed on a dilatometer model DIL 420 from Netzsch, with a maximum temperature of 1200 °C and a heating rate of 5 °C $min^{-1}$ in air atmosphere. The relative density values were obtained for each composition from the geometrical (apparent density = mass/volume) and theoretical densities (Eq. (1)). Microstructural characterization of polished and thermally etched (25 °C below the firing temperature) samples was carried out by scanning electron microscopy (LEO, model 1430). To evaluate the average grain size, approximately 200 grains were measured in each sample. The measured values were organized in a histogram and the distribution was refined using a *Gaussian* function. The electrical characterization of samples sintered at 1050 °C for 5 h was performed by impedance spectroscopy (IS) using an inconel 600 sample holder with Pt contact leads and a K-type thermocouple placed near the specimens. Silver contacts were painted on the parallel faces of samples and cured at 600 °C. Electrical measurements were carried out in the temperature range 200–600 °C in static ambient atmosphere using a Solartron (model 1260) impedance analyzer. The IS data were collected with increasing temperature after stabilizing the sample (~ 30 min) at selected measuring temperatures. The frequency ranged from 0.1 Hz to 15 MHz with a signal amplitude of 0.1 V. The IS data were analyzed using the ZView program (Scribner Associates, Inc.).

## 3. Results and discussion

TG/DTA curves of selected precursor powders of nominal composition $Ce_{0.99-x}Gd_xCu_{0.01}O_{2-\delta}$ (x = 0; 0.1; 0.20; and 0.30) show three stages of thermal decomposition, as depicted in Fig. 1. The endothermic peak between 30 and 150 °C, with mass loss of 3–5%, is related to the desorption of physically adsorbed water. The second stage of thermal decomposition, occurring between 200 and 450 °C, is related to the burning of organics from the chemical synthesis. The enthalpy change, characterized by the exothermic peak, suggests that increasing the

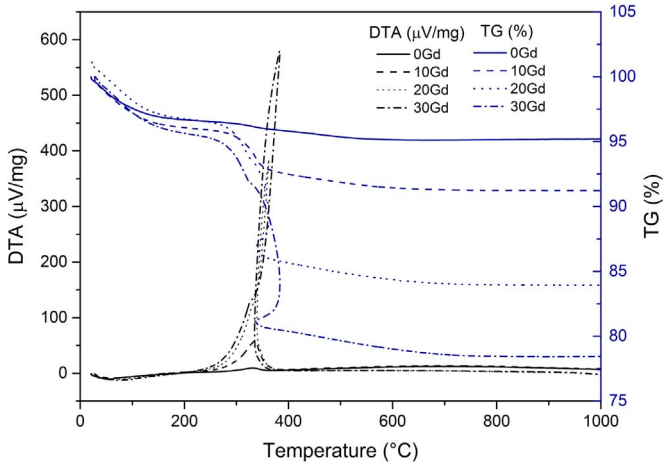


**Fig. 1.** TG/DTA curves of precursor powders of composition $Ce_{0.99-x}Gd_xCu_{0.01}O_{2-\delta}$ (x = 0; 0.1; 0.20; and 0.30).

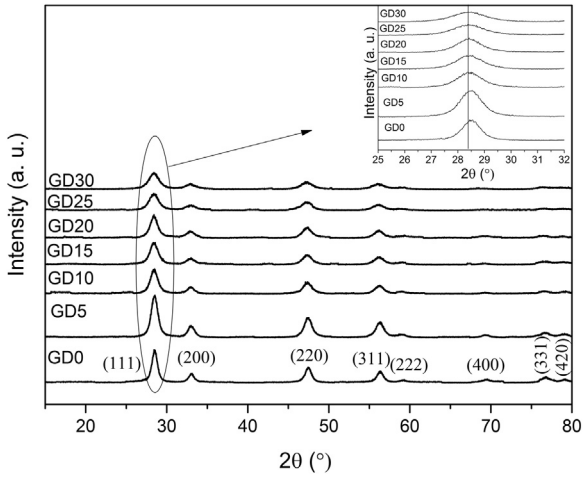


**Fig. 2.** Powder X-ray diffractograms for samples with different gadolinium content. The inset shows the shift of the peak corresponding to the plane (111).

**Table 1**
Crystallographic parameters and refinement indexes for compositions $Ce_{0.99-x}Gd_xCu_{0.01}O_{2-\delta}$ calcined at 500 °C.

| Composition (x) | *Crystallographic parameters* | | | | | |
|---|---|---|---|---|---|---|
| | ***a = b = c (nm)*** | ***Volume (Å)*** | $D_{XRD}$ ***(nm)*** | $R_{wp}$ ***(%)*** | $R_{exp}$ ***(%)*** | $\chi^2$ |
| 0 | 0.5411(6) | 158.48(3) | 16.78 | 9.71 | 8.24 | 1.18 |
| 0.05 | 0.5418(6) | 159.09(6) | 14.43 | 7.94 | 7.43 | 1.07 |
| 0.10 | 0.5418(6) | 159.09(2) | 12.61 | 11.08 | 8.10 | 1.37 |
| 0.15 | 0.5421(1) | 159.31(8) | 11.33 | 9.41 | 8.27 | 1.14 |
| 0.20 | 0.5425(1) | 159.67(0) | 11.88 | 10.47 | 8.15 | 1.29 |
| 0.25 | 0.5436(8) | 160.70(2) | 10.04 | 8.55 | 8.39 | 1.02 |
| 0.30 | 0.5439(7) | 160.93(8) | 8.87 | 8.50 | 7.04 | 1.21 |

content of gadolinium nitrate accentuates the exothermic character of the combustion reaction. Mass losses ranged from 5% for a gadolinium-free composition to 22% for a composition with Gd content x = 0.30. The third stage of thermal decomposition (> 400 °C) can be attributed to the oxidation of residual organic matter, followed by crystallization of ceria-based solid solutions. The obtained powders were then calcined at 500 °C for 1 h to achieve a nanocrystalline powder.

The XRD patterns of calcined powders (Fig. 2) confirm the ceria cubic fluorite-type structure in the entire composition range. Within the detection limit of XRD, no evidence of secondary phases was observed,

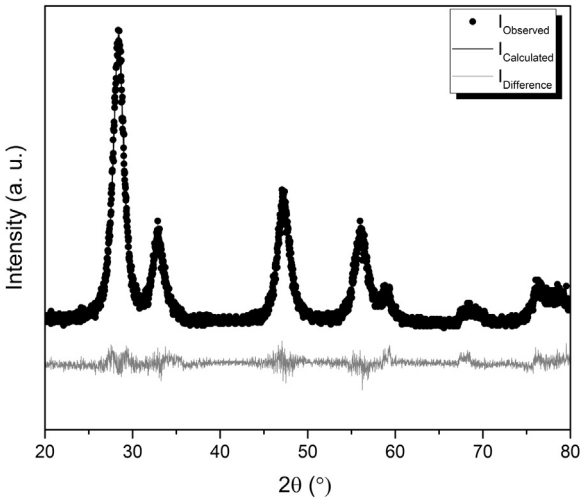


**Fig. 3.** X-ray patterns (observed, calculated and difference) of $Ce_{0.89}Gd_{0.1}Cu_{0.01}O_{1.94}$.

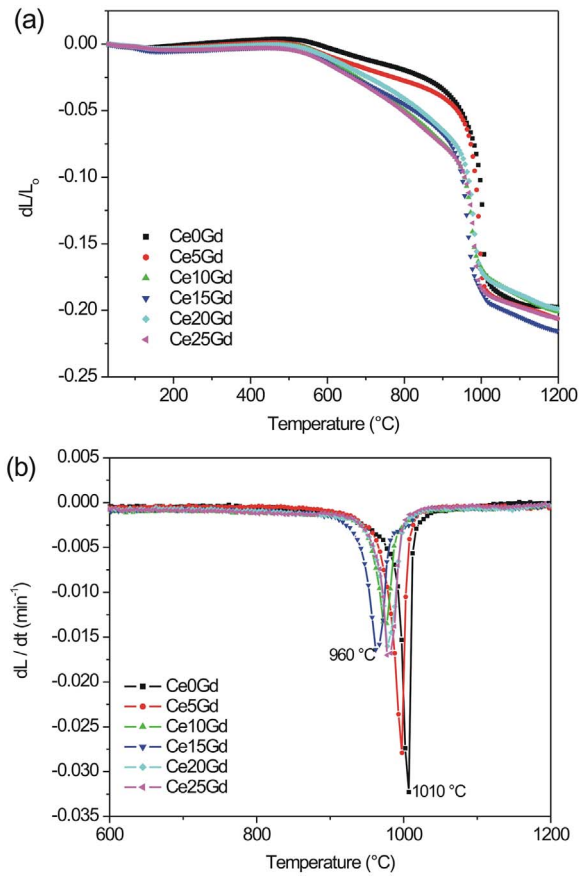


**Fig. 4.** Curves of (a) linear shrinkage and (b) linear shrinkage rate of samples with different gadolinium contents.

**Table 2**
Theoretical density values calculated from lattice parameters.

| Theoretical density (g cm$^{-3}$) | $Ce_{0.99-x}Gd_xCu_{0.01}O_{2-\delta}$ | | | | | | |
|---|---|---|---|---|---|---|---|
| | **0** | **0.05** | **0.10** | **0.15** | **0.20** | **0.25** | **0.30** |
| | 7.29(7) | 7.28(8) | 7.30(7) | 7.31(6) | 7.31(8) | 7.29(0) | 7.32(1) |

**Table 3**
Relative density values as a function of composition $Ce_{0.99-x}Gd_xCu_{0.01}O_{2-\delta}$ and sintering temperature.

| Temperature (°C) | Relative density (%) Composition x | | | | | | |
|---|---|---|---|---|---|---|---|
| | 0 | 0.05 | 0.10 | 0.15 | 0.20 | 0.25 | 0.30 |
| 950 | 76.86 | 74.25 | 72.05 | 70.84 | 67.30 | [a] | 67.73 |
| 1000 | 76.73 | 70.03 | 71.00 | 71.81 | 72.71 | 73.50 | 86.80 |
| 1050 | 91.78 | 96.83 | 91.67 | 91.55 | 92.22 | 87.03 | 97.56 |

[a] Sample damaged during handling.

suggesting that $Cu^{2+}$ and $Gd^{3+}$ contents did not exceed the limit of solubility in the ceria lattice. Fig. 2 indicates that the gadolinium content exerts an effect on the diffraction peaks. Such an effect is observed as a shift of the main peak, plane (111), towards smaller 2θ angles with increasing gadolinium content, as seen in the inset of Fig. 2. These results confirm the replacement of $Ce^{4+}$ ions, by $Gd^{3+}$ (with ionic radius larger than $Ce^{4+}$), forming solid solutions of Ce-Gd-Cu-O. The increased Gd-content produces a progressive increase of oxygen vacancies that induces a broadening of the diffraction peaks and an increase of the lattice parameter [15,16].

Table 1 summarizes the lattice parameter (nm), unit cell volume (Å$^3$), $D_{XRD}$ crystallite size (nm) and refinement indexes ($R_{wp}$, $R_{exp}$, $\chi^2$), obtained by Rietveld refinement [17]. The good quality of the Rietveld refinements can be evaluated by the values of the $\chi^2$ index. The refined parameters indicate that the lattice constant for 1 mol% Cu (sample $Ce_{0.99}Cu_{0.01}O_{2-\delta}$) is close to that of pure ceria (a = 0.5411 nm, JCPDS 43-1002). For the solid solutions with increasing Gd content, both the lattice constant and the unit cell volume increase. This expansion of the structure is due to the difference between the ionic radius of $Gd^{3+}$ (0.105 nm) and $Ce^{4+}$ (0.097 nm) with coordination VIII [18]. The incorporation of the larger trivalent ion causes a distortion in the ceria structure. The crystallite sizes ($D_{XRD}$ = 8–16 nm) are lower than typically reported values for powders obtained by combustion (40–50 nm) [19] and citrate complexation methods (53 nm) [20], both with calcination conditions similar to that used in the present study. It is important to mention that small crystallite/particle sizes tend to increase the sinterability of ceramics, decreasing the temperature required for maximum densification due to the increased surface area. Graphical evidence of the good refinement quality is shown in Fig. 3.

Fig. 4 shows the effect of gadolinia content on the sintering behavior (linear shrinkage and shrinkage rate) of green samples. The linear shrinkage curves (Fig. 4a) indicate the onset of the mass transport at ~ 500 °C, followed by two distinct retraction stages with increasing temperature that characterize different sintering mechanisms. The sintering stage between ~ 560 and 900 °C may be associated with solid state diffusion (grain boundary diffusion, surface and volumetric diffusion [12]). The mechanism associated with the sintering stage occurring between 950 and 1050 °C may be associated with the formation of liquid phase, possibly composed of a ternary phase of $Gd_2O_3$-$CeO_2$-CuO [21], promoting a rapid densification due to diffusion of matter under the capillary action on surface of the grains [22]. This liquid phase is promoted by the incorporation of CuO, which has a lower melting point (1326 °C) than those of $CeO_2$ (2400 °C) and $Gd_2O_3$ (2420 °C), decreasing the total melting point of the ternary composition. According to Lima et al. [23], gadolinium-doped ceria (CGO) co-doped with 1 mol% CuO begins to shrink at approximately 600 °C, while CuO-free CGO samples begins shrinkage at approximately 1000 °C.

The shrinkage rate for all compositions is depicted in Fig. 4b. The temperature for a maximum shrinking rate is lower for the composition x = 0.15. In contrast, in the Gd-free sample the maximum shrinkage rate temperature occurs at the highest measured T = 1010 °C, indicating the effect of Gd on the sintering of the ceramic. According to Inaba et al. [24], the densification of the ceramic occurs due to the retraction/removal of pores and, consequently, through the release of oxygen gas contained inside the pores. Hence, the diffusion rate of oxygen through the ceramic is crucial for a higher densification rate, with a higher densification rate promoted by a higher mobility of the $O^{2-}$ ion [24]. With increasing Gd content there is an increase the amount of oxygen vacancies; however, due to the association effect between oxygen vacancies and doping cations, the vacancy mobility at high dopant concentrations is decreased, leading to impaired ceria sinterability for high dopant concentrations. In this work, this effect was found for samples containing Gd contents greater than x = 0.2. As the lowest temperature of maximum shrinkage rate was found for the sample of composition x = 0.15, this is the best composition from the point of view of sintering. The sample x = 0.30 is not shown because it follows the trend of composition x = 0.25. To evaluate the effects of

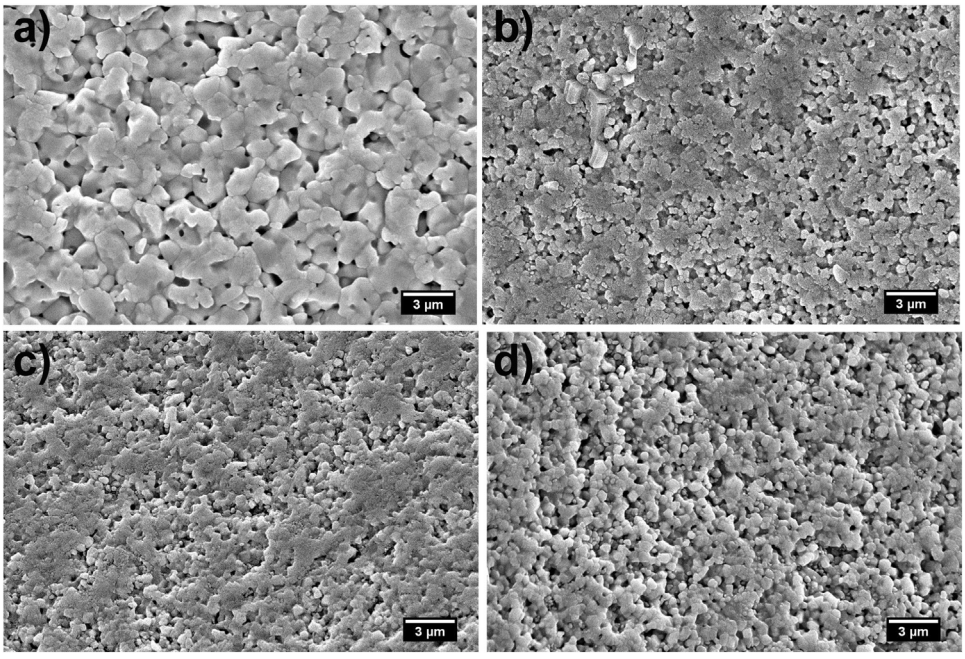


**Fig. 5.** SEM cross-section images of samples $Ce_{0.99-x}Gd_xCu_{0.01}O_{2-\delta}$ (a) x = 0, (b) x = 0.10, (c) x = 0.15, and (d) x = 0.20 sintered at 1050 °C.

**Table 4**
Equivalent grain average diameter of sintered samples $Ce_{0.99-x}Gd_xCu_{0.01}O_{2-\delta}$.

| Sample | Composition x | | | | |
|---|---|---|---|---|---|
| | **0** | **0.10** | **0.15** | **0.20** | **0.3** |
| Average grain size (μm) | 1.630 ± 0.427 | 0.372 ± 0.152 | 0.345 ± 0.149 | 0.340 ± 0.145 | 0.113 ± 0.034 |

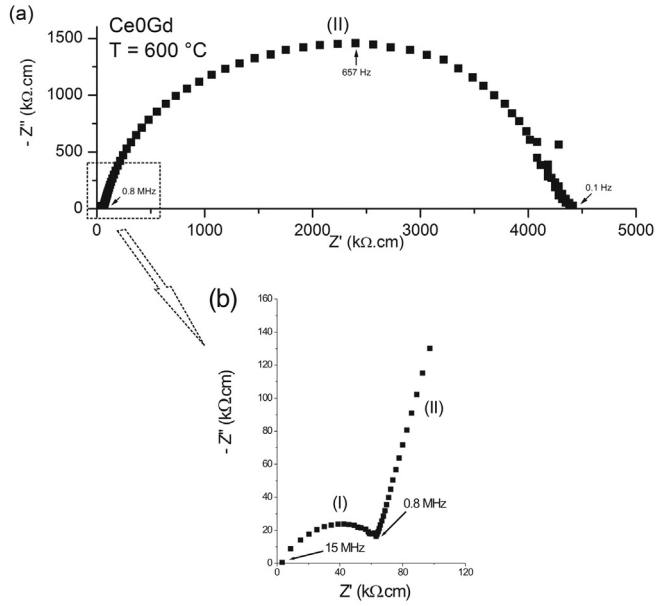


**Fig. 6.** Impedance spectrum of the $Ce_{0.99}Cu_{0.01}O_{2-\delta}$ composition acquired at 600 °C; (a) full view and (b) high-frequency view.

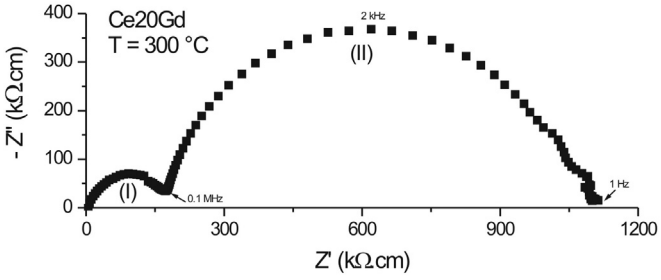


**Fig. 7.** Impedance spectrum at 300 °C for sample the sample x = 0.20 (I) corresponds to grain contribution and (II) to grain boundary contribution.

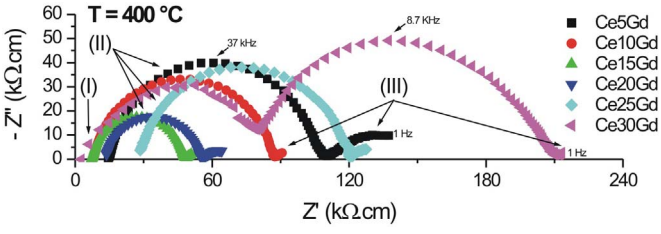


**Fig. 8.** Impedance spectra obtained at 400 °C for samples $Ce_{0.99-x}Gd_xCu_{0.01}O_{2-\delta}$, x = 0.05 to x = 0.30.

sintering temperature and Gd content on the relative density, samples of composition $Ce_{0.99-x}Gd_xCu_{0.01}O_{2-\delta}$ (x = 0; 0.05; 0.10; 0.15; 0.20; 0.25; 0.30) were sintered at 950, 1000 and 1050 °C. By applying the lattice parameters from Rietveld refinement to Eq. (1), one obtains the theoretical densities shown in Table 2. The relative density values calculated from the theoretical and geometric densities, are presented in Table 3.

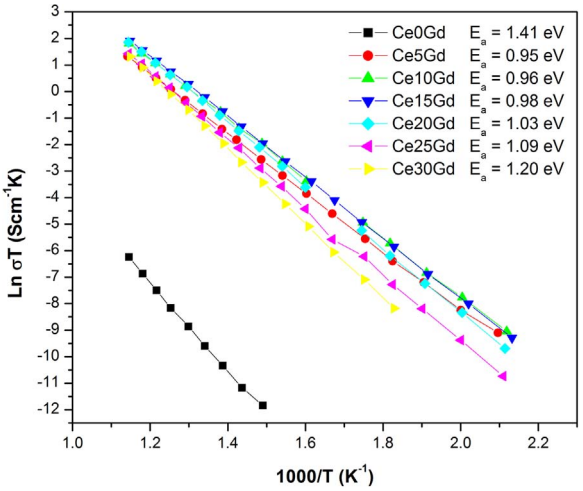


**Fig. 9.** Arrhenius plots of the total conductivities for samples $Ce_{0.99-x}Gd_xCu_{0.01}O_{2-\delta}$, x = 0.05 to x = 0.30.

The results show an increase in relative density with increasing sintering temperature, as expected. For the highest sintering temperature used in the current study (1050 °C), the relative densities of most of the studied compositions are ~ 91%. These relative density values are consistent with the microstructures presented in Fig. 5. In addition to evidence of slight porosity, it is also possible to observe that the average grain size decreases with the addition of gadolinia, as listed in Table 4.

The electrical characterization by impedance spectroscopy was performed in samples sintered at 1050 °C for 5 h. Fig. 6 shows a typical IS diagram obtained at 600 °C for the composition $Ce_{0.99}Cu_{0.01}O_{2-\delta}$ (Ce0Gd). Two semicircles are identified: a small component at high frequency and a major contribution at lower frequencies, which are related to the conduction processes occurring at the bulk (I - Fig. 6b) and the blocking of oxygen ions (II - Fig. 6a and b), respectively. As can be observed, the sample is highly resistive, mainly due to the low frequency component, which reflects the contribution of both grain boundary and other blocking mechanisms such as pores. Such a feature is consistent with the microstructure and density of the CuO-doped ceria without gadolinia.

The IS data measured at 300 °C for sample x = 0.20 (Ce20Gd) is shown in Fig. 7. Decreasing the temperature from 600 to 300 °C results in a rapid increase of the resistance associated with both high and low frequencies, characteristic of the thermally activated conduction of oxygen ions in ceria-based materials. The measured IS diagrams were fitted to electrical circuits comprised of parallel RC (Resistor/Constant phase element) elements connected in series. For measuring temperatures above 400 °C the grain bulk semicircle tends to disappear within the frequency range of the measurement as the grain becomes very conductive with related low time constant. The same happens for the grain boundary (above 600 °C) leaving only the electrode response visible.

Fig. 8 shows impedance spectra obtained at 400 °C for samples with different Gd contents. It is observed that the grain response can be simulated by a simple resistor, with the complete grain response not being observable in the frequency window of the measurement. In addition, it is also possible to observe (for some samples) the beginning

**Table 5**
Literature survey on electrical properties and on own data on ceria-based solid electrolytes.

| Composition | $\sigma_{500}$ (S cm$^{-1}$) | $\sigma_{600}$ (S cm$^{-1}$) | Activation energy (eV) | Reference |
|---|---|---|---|---|
| $Ce_{0.99}Cu_{0.01}O_{2-\delta}$ | $3.56 \times 10^{-7}$ | $2.23 \times 10^{-6}$ | 1.41 | This work |
| $Ce_{0.94}Gd_{0.05}Cu_{0.01}O_{2-\delta}$ | $9.28 \times 10^{-4}$ | $4.31 \times 10^{-3}$ | 0.95 | This work |
| $Ce_{0.89}Gd_{0.10}Cu_{0.01}O_{2-\delta}$ | $1.59 \times 10^{-3}$ | $7.03 \times 10^{-3}$ | 0.96 | This work |
| $Ce_{0.84}Gd_{0.15}Cu_{0.01}O_{2-\delta}$ | $1.72 \times 10^{-3}$ | $7.81 \times 10^{-3}$ | 0.98 | This work |
| $Ce_{0.79}Gd_{0.20}Cu_{0.01}O_{2-\delta}$ | $1.54 \times 10^{-3}$ | $7.33 \times 10^{-3}$ | 1.03 | This work |
| $Ce_{0.74}Gd_{0.25}Cu_{0.01}O_{2-\delta}$ | $8.47 \times 10^{-4}$ | $4.77 \times 10^{-3}$ | 1.09 | This work |
| $Ce_{0.69}Gd_{0.30}Cu_{0.01}O_{2-\delta}$ | $6.52 \times 10^{-4}$ | $4.27 \times 10^{-3}$ | 1.21 | This work |
| $CeO_{2-\delta}$ | – | $1.1 \times 10^{-5}$ | 1.03 | [23] |
| $Ce_{0.80}Sm_{0.20}O_{2-\delta}$ | – | $6 \times 10^{-3}$ | 0.94 | [25] |
| $Ce_{0.80}Sm_{0.20}O_{2-\delta}$ | $5.35 \times 10^{-4}$ | – | 0.73 | [26] |
| $Ce_{0.89}Gd_{0.10}Cu_{0.01}O_{2-\delta}$ | – | $15.5 \times 10^{-3}$ | – | [19] |
| $Ce_{0.79}Gd_{0.20}Zn_{0.01}O_{2-\delta}$ | – | $18 \times 10^{-3}$[a] | 0.71 | [29] |
| $Ce_{0.79}Gd_{0.20}Cu_{0.01}O_{2-\delta}$ | – | $26 \times 10^{-3}$ | 1.164 | [30] |

[a] Measured at 650 °C.

of a semicircle at high frequency related to processes that occur at the interface between the ceramics and the porous platinum electrodes (III), marking the limit of grain boundary response and start of the electrode response. The IS data in Fig. 8 indicate that the resistivity of the samples decreases with increasing the Gd content, that may be related to the formation of oxygen vacancies due to increasing dopant concentration. However, the resistivity increases for $x > 0.20$, which may be related to the formation of dopant ion/oxygen vacancy clusters. Such clusters reduce the mobility of the vacancies and, thus, electrical conductivity. In addition, the decrease in conductivity may be related to the increase in grain boundary density that also decreases the vacancy mobility, as well as the presence of pores.

The Arrhenius plots of the total conductivity for the studied compositions are shown in Fig. 9. The sample with the lowest conductivity values, in the temperature range of 400–600 °C, is the gadolinia-free composition ($Ce_{0.99}Cu_{0.01}O_{2-\delta}$), in good agreement with the low conductivity of pure ceria, considered a poor ionic conductor ($\sigma_{700\,°C} = 1.9 \times 10^{-5}$ S cm$^{-1}$) [23]. Improved conductivity is observed after addition of small amounts of gadolinia ($x = 0.05$). The maximum conductivity is found for samples $x = 0.10$–$0.15$. In all samples, doping with Gd generates oxygen vacancies that maintain the electrical neutrality of the ceria lattice and permit oxygen ionic conduction [26].

A comparison of electrical properties of the herein studied ceria-based solid solutions with literature data is shown in Table 5. The values of conductivity increase with the addition of $Gd^{3+}$ cations, reaching a maximum of 7.81 mS cm$^{-1}$ at 600 °C for the sample $x = 0.15$. This result represents an improvement compared to a CuO free sample containing 20 atm.% Sm and sintered at 1500 °C for 5 h (6 mS cm$^{-1}$ at 600 °C, relative density greater than 95%) [27]. Considering samples with the similar dopant contents (20 atm.% Gd or Sm), the current conductivities measured at 500 and 600 °C are higher than literature reports for samples sintered at 1275 °C [28] and 1500 °C [27]. The activation energy (Ea) values, ranging from 0.95 to 1.41 eV, are in line with those of doped ceria compositions from literature, as shown in Table 5 and Fig. 9. The increasing values of Ea with Gd-content can be related to an increasing amount of local order, where positively charged oxygen vacancies and negatively charged Gd substitutions combine to form ordered clusters, thus, requiring an increased dissociation energy for ionic conduction [31].

## 4. Conclusions

Nanocrystalline particles of ceria-based solid solutions $Ce_{0.99-x}Gd_xCu_{0.01}O_{2-\delta}$ ($x = 0$; 0.05; 0.10; 0.15; 0.2; 0.25 and 0.30) were successfully obtained by the polymeric precursor method. The association of two processing methodologies (nanoparticles and sintering aid) allowed the attainment of ceramics with relatively dense microstructures after sintering at 1050 °C. Co-doping with $Gd_2O_3$ favored densification and decreased the sintering temperature by ~ 50 °C. Both the gadolinium content and ceramic microstructure affect the electrical conductivity, with smaller grains resulting in lower total conductivity. Overall results indicate that Cu and Gd co-doped ceria sintered at 1050 °C is a promising material for application as solid oxide fuel cell electrolyte.

## Acknowledgements

The authors acknowledge CNPq (447797/2014-0, 311883/2016-8 and 447813/2014-5), FAPESP (2014/09087-4 and 2014/50279-4) and FCT (Portugal) for the financial support. Thamyscira H. Santos thanks CAPES (Coordenação de Aperfeiçoamento de Nível Superior, Brazil) for the MSc Grant.

## References

[1] H.J. Koch, Challenges of implementing new technologies for sustainable energy opening address at the Sixth Grove Fuel Cell Symposium, London, 13-16 September 1999, J. Power Sources 86 (2000) 2–8.
[2] A.B. Stambouli, Fuel cells: the expectations for an environmental-friendly and sustainable source of energy, Renew. Sustain Energy Rev. 15 (2011) 4507–4520.
[3] T. Elmer, M. Worall, S. Wu, S.B. Riffat, Fuel cell technology for domestic built environment applications: state of-the-art review, Renew. Sustain. Energy Rev. 42 (2015) 913–931.
[4] A. Choudhury, H. Chandra, A. Arora, Application of solid oxide fuel cell technology for power generation – a review, Renew. Sustain. Energy Rev. 20 (2013) 430–442.
[5] O. Yamamoto, Solid oxide fuel cell: fundamental aspect and prospects, Electrochem. Acta 45 (2000) 2423–2435.
[6] S.C. Singhal, K. Kendall, High Temperature Solid Oxide Fuel Cells: Fundamentals, Design and Applications, Elsevier, Amsterdan, 2006.
[7] J. Larminie, A. Dicks, Fuel Cell Systems Explained, John Wiley & Sons LTD, Chichester, 2003.
[8] R. Chiba, Síntese, processamento e caracterização das meia-células de óxido sólido catodo/eletrólito de manganito de lantânio dopado com estrôncio/zircônia estabilizada com ítria, Instituto de Pesquisas Energéticas e Nucleares - IPEN, São Paulo, Brasil, 2010.
[9] M.A.F. Oksuzomer, G. Donmez, V. Sariboga e, T.G. Altinçekiç, Microstructure and ionic conductivity properties of gadolinia doped ceria ($Gdx_Ce1_{-xO}2_{-x/2}$) electrolytes for intermediate temperature SOFCs prepared by the polyol method, Ceram. Int. 39 (2013) 7305–7315.
[10] J.W. Fergus, Electrolytes for solid oxide fuel cells, J. Power Sources 162 (2006) 30–40.
[11] J.M.G. Martínez, Obtenção de Eletrólitos Sólidos Com Composição Ce0,8Gd0,2O1,9, Para Aplicações em Células a Combustível, Universidade de Brasília, Brasil, 2013.
[12] Y. Dong, S. Hampshire, J. Zhou, G. Meng, Synthesis and sintering of Gd-doped CeO2 electrolytes with and without 1 at% CuO doping for solid oxide fuel cell applications, Int. J. Hydrog. Energy 36 (2011) 5054–5066.
[13] D. Fagg, J. Abrantes, D. Pérez-Coll, P. Núñez, V. Kharton, J. Frade, The effect of cobalt oxide sintering aid on electronic transport in $Ce_{0.80}Gd_{0.20}O_{2-\delta}$ electrolyte, Electrochim. Acta 48 (2003) 1023–1029.
[14] D. Fagg, V. Kharton, J. Frade, Transport in ceria electrolytes modified with sintering aids: effects on oxygen reduction kinetics, J. Solid State Electrochem. 8 (2004) 618–625.
[15] B.Z. Matovic, D.M. Bucevac, M. Rosic, B.M. Babic, Z.D. Dohcevic-Mitrovic, M.B. Radovic, Z.V. Popovic, Synthesis and characterization of Cu-doped ceria

nanopowders, Ceram. Int. 37 (2011) 3161–3165.
[16] G.S. Godoi, D.P.F. Souza, Efeito de íon aliovalentes nas propriedades elétricas de céria dopada com ítria, Matéria 13 (2008) 512–521.
[17] M.J.C. Oliveira, M.R. Quirino, L.S. Neiva, L. Gama, J.B. Oliveira, Síntese de óxido de cério (CeO2) com alta área superficial por meio do método hidrotérmico assistido por microondas, Rev. Eletron. Mater. Proces. 6 (2011) 170–174.
[18] B. Cela, D.A. Macedo, G.L. Souza, A.E. Martinelli, R.M. Nascimento, C.A. Paskocimas, NiO-CGO in situ nanocomposite attainment: one step synthesis, J. Power Sources 196 (2011) 2539–2544.
[19] R.V. Wandekar, M. Ali, B.N. Wani, S.R. Bharadwaj, Physicochemical studies of NiO-GDC composites, Mater. Chem. Phys. 99 (2006) 289–294.
[20] R.O. Fuentes, R.T. Baker, Structural, morphological and electrical properties of Gd0,1Ce0,9O1,95 prepared by a citrate complexation method, J. Power Sources 186 (2009) 268–277.
[21] C.G.M. Lima, T.H. Santos, J.P.F. Grilo, R.P.S. Dutra, R.M. Nascimento, S. Rajesh, F.C. Fonseca, D.A. Macedo, Synthesis and properties of CuO-doped Ce0.9Gd0.1O2-δ electrolytes for SOFCs, Ceram. Int. 41 (2014) 4161–4168.
[22] Y. Xia, Y. Bai, X. Wu, D. Zhou, Z. Wang, X. Liu, J. Meng, Effect of sintering aids on the electrical properties of Ce0.9Nd0.1O2-δ, Solid State Sci. 14 (2012) 805–808.
[23] R.A. Rocha, E.N.S. Muccillo, Efeito da temperatura de calcinação e do teor de dopante nas propriedades físicas da céria-gadolínia preparada pela complexação de cátions com ácido cítrico, Cerâmica 47 (2001) 219–224.
[24] H. Inaba, T. Nakajima, H. Tagawa, Sintering behaviors of ceria and gadolinia-doped ceria, Solid State Ion. 106 (1998) 263–268.
[25] W. Huang, P. Shuk, M. Greenblatt, Hydrothermal synthesis and properties of Ce1-xSmxO2-x/2 and Ce1-xCaxO2-x solid solutions, Chem. Mater. 9 (1997) 2240–2245.
[26] K. Huang, M. Feng, J. Goodenough, Synthesis and electrical properties of dense $Ce0.9Gd0.1O1.9_5$ ceramics, J. Am. Ceram. Soc. 81 (1998) 357–362.
[27] R. Peng, C. Xia, Q. Fu, G. Meng, D. Peng, Sintering and electrical properties of (CeO2)0.8(Sm2O3)0.1 powders prepared by glycine-nitrate process, Mater. Lett. 56 (2002) 1043–1047.
[28] M. Srivastava, K. Kumar, N. Jaiswal, N.K. Singh, D. Kumar, O. Parkash, Enhanced ionic conductivity of co-doped ceria solid solutions and applications in IT-SOFs, Ceram. Int. 40 (2014) 10901–10906.
[29] L.A. Villas-Boas, F.M. Figueiredo, D.P.F. Souza, F.M.B. Marques, Zn as sintering aid for ceria-based electrolytes, Solid State Ion. 262 (2014) 522–525.
[30] Y. Dong, S. Hampshire, B. Lin, Y. Ling, X. Zhang, High sintering activity Cu-Gd co-doped CeO2 electrolyte for solid oxide fuel cells, J. Power Sources 195 (2010) 6510–6515.
[31] J. Faber, C. Geoffroy, A. Roux, A. Sylvestre, P. Abélard, A systematic investigation of the dc electrical conductivity of rare-earth doped ceria, Appl. Phys. A 49 (1989) 225–232.